IEEE Access
Multidisciplinary | Rapid Review | Open Access Journal

Received 16 September 2023, accepted 24 September 2023, date of publication 4 October 2023,
date of current version 11 October 2023.

Digital Object Identifier 10.1109/ACCESS.2023.3321842

APPLIED RESEARCH

Flexibility in Hexapod Robots: Exploring Mobility of the Body

RAFAEL PEREIRA BACHEGA[1,2], GABRIEL PEREIRA DAS NEVES[1,3], ALEXANDRE BRINCALEPE CAMPO[2], AND BRUNO AUGUSTO ANGELICO[1]

[1]Department of Telecommunications and Control Engineering, Escola Politécnica, University of São Paulo, São Paulo 05508-010, Brazil
[2]Department of Electrical Engineering, Federal Institute of São Paulo, São Paulo 01109-010, Brazil
[3]Department of Engineering, Insper Learning Institution, São Paulo 04546-042, Brazil

Corresponding author: Rafael Pereira Bachega (rafaelbachega@usp.br)

This work was supported in part by Coordenação de Aperfeiçoamento de Pessoal de Nível Superior (CAPES) under Grant 001; and in part by Conselho Nacional de Desenvolvimento Científico e Tecnológico (CNPq), Brazil, under Grant 308356/2021-7.

ABSTRACT Introducing Myrmex, a hexapod robot designed for autonomous locomotion on unstructured terrains. It was developed a whole-body kinematics model that enables both open-chain and closed-chain control of the robot. This model enhances the flexibility and mobility of the robot. At the moment, Myrmex relies solely on proprioception (encoders and IMU) for adapting its body posture. Despite these sensory limitations, we have successfully applied the model in static and dynamic situations. Static experiments have showcased increased flexibility, allowing the robot to access previously challenging locations. In dynamic scenarios, the hexapod has demonstrated its capability to traverse irregular terrains, effectively exploiting its body mobility. Myrmex adeptly adjusts its posture according to the terrain topology, maintaining the center of gravity projection along the body's centerline (i.e., same as it in the level walk), thus preserving stability margins during gait. The robot was able to correct its posture on terrain with gradients in any direction relative to the body structure, with only 3 DoF per leg. Importantly, our experiments have underscored the robot's ability to maintain its posture even in the face of unexpected disturbances in its legs, emphasizing the robustness and reliability of the model.

INDEX TERMS Hexapod robot, autonomous locomotion, proprioception, body posture, whole-body kinematic control, stability margin.

I. INTRODUCTION

Traverse rough terrain with careful foot placement and control, beyond the ability to overcome obstacles, makes locomotion with legs admirable. Many living beings use their legs with great flexibility concerning behavioral requirements and avail these maneuvers when using body mobility [1]. Insects and other arthropods, in particular, have a set of unspecialized walking legs. These limbs are recruited into various adaptive locomotion and manipulation behaviors such as moving in confined spaces [2], climbing [3], [4], [5], pulling loads [6], carrying food [7], [8], crossing gaps and overcome obstacles [9], [10]. The locomotion behaviors exemplified are flexible in that the leg joints coordination must be adjusted to provide a particular goal. Likewise, mobility and adaptability in legged robots directly correlate with their workspace, considering the geometry and degrees of freedom (DoF) of the legs. Despite attractive properties, legged robots have their limitations. Designing control algorithms for these hardware platforms remains a challenge. From the control perspective, these robots are high-dimensional and non-smooth systems with many physical constraints [11]. In practice, these restrictions lead to substantial compromises in performance, such as slow acceleration [12], a fixed upright pose of the body, and limited velocity of the limbs [13]. The contact points change over time depending on the maneuver being performed and, therefore, cannot be prespecified [14]. Considering the whole-body in the operational space of tasks, the transition from one posture to another is an activity sensitive to the

The associate editor coordinating the review of this manuscript and approving it for publication was Yangmin Li.

accumulation of uncertainties in actuation [15]. A complex set of sensors and multiple layers of software cause noise and latencies in the transfer of information [16]. This evidence shows how robots with legs still represent one of the more challenges in robotics.

A. RELATED WORKS

Recent research shows great interest in behavioral analysis during locomotion in multi-legged robots. ANYmal [17], [18] demonstrated smooth gaits transition and agile locomotion outdoors based on a simplified model with a hierarchical whole-body controller. Using only proprioceptive information, the robot HyQ [19] can detect, estimate and recover from slip conditions. The Cheetah 3 robot, developed at MIT [20], focused on situations where the robot body is underactuated. This robot can stabilize gaits with complex orientation dynamics, such as jumps or gallops, without using exteroceptive sensors. Although LittleDog [21] achieved impressive results, and until now, this remains state of the art for rough-terrain locomotion, the progress of six-legged robots could perform better in unstructured terrain. Hexapod robots have advantages over bipeds or quadrupeds in static stability during walking [22], and currently there are few relevant hardware implementations of these mechanisms.

Hexapod robots such as DLRCrawler, Messor II and AMOS II [23], [24], [25] explored their locomotion using the open chain kinematic model, being able to control the leg's position but not the body's posture. The RHex robot [26], [27] started locomotion on uneven terrain using biological principles with reduced degrees of freedom (1 DoF per leg). Although capable of achieving remarkable mobility, RHex cannot select individual contact points [28] or optimize your posture [29] (which is essential on rough terrain). Weaver and Lauron V robots can adjust the position and orientation of their legs to correct their body posture and improve locomotion on sloped terrain. However, to achieve greater flexibility and adaptability in these robots, it was necessary to increase the number of degrees of freedom in their platforms. The Lauron V robot, for instance, used 4 DoF in each leg [30] to adapt its posture in the longitudinal direction. Weaver [31] addressed the problem by expanding to 5 DoF on each leg to adapt to other orientations.

B. CONTRIBUTION

This article introduces an approach that relies exclusively on proprioception for controlling locomotion and adapting body posture in hexapod robots. While previous research and significant studies [23], [24], [25], [26], [27], [28], [29] have focused only on leg kinematics and contributed significant advances to the field, our model considers the kinematics of the whole-body. This approach enables locomotion strategies that, to the best of the authors' knowledge, have not been presented in other hexapod robots, unlike previous works that adapt posture on uneven surfaces using exteroceptive sensors [32], [33], [34]. Exteroceptive sensors, such as cameras, LIDARs, and structured light, demand well-lit, opaque, textured, and highly structured environments, which are not always achievable in real scenarios. Therefore, this work provides the following contributions: firstly, a kinematic model for multi-legged robots was introduced, which adjusts the body posture to preserve the stability margin during walking. The mathematical model of a multi-legged robot is not universal or unified. We propose a posture adaptation solution considering legs in open and closed kinematic chains. Secondly, it has been validated that legs with only 3 DoF are sufficient to handle gradients in any direction relative to the body and on uneven terrain. Practical experiments conducted on the hexapod robot named Myrmex demonstrate that the adaptability of the body in relation to the terrain considerably enhanced the autonomy and resilience of the robot compared to prior outcomes [35], rendering it well-suited for demanding scenarios.

Extensive experiments were carried out, and our method was assessed. Although Myrmex lacks impedance control or vision systems, we aim to enable the robot to deal with the problems in a real behavioral context. Two sets of experiments are presented. In the first set, only static situations will be considered. The robot's whole-body model is explored to increase its flexibility (task space) by using body posture to reach places that would otherwise be kinematically infeasible with leg control alone. In the second set, we forced Myrmex to walk on uneven terrain to explore the mobility of its body. The types of geometric features chosen for the study include gradients and steps that are compatible with the robot's dimensions.

The remainder of this paper is organized in this way: Section II presents the model for whole-body kinematic control. The Section III describes the robot architecture along with the validation of the developed model. Differences between flexibility and mobility in legged robots are described in Section IV. Section V presents the experimental evaluation of the proposed whole-body kinematics in static situations. Adaptive body behaviors and their experimental evaluation in locomotion are reported in Section VI. The limitations and comparisons are discussed in Section VII. At the end of the article, Section VIII contains the conclusion and future proposals.

II. MODEL FORMULATION

Walking robots belong to the class of floating base systems, that is, systems that are not rigidly connected to their environment and can move anywhere in the workspace using the ground as support [17]. Each leg remains in one of two possible mutually exclusive states - stance (support phase) or swing (transfer phase). The legs during stance (period in contact with the surface) form the closed chain system, and the legs in the swing phase (period in which they are not in contact with the surface) represent the open chain system. There is mechanical coupling only in the closed chain [36]. Locomotor control strategies with gait and posture motions for the two systems must be completely different. This section

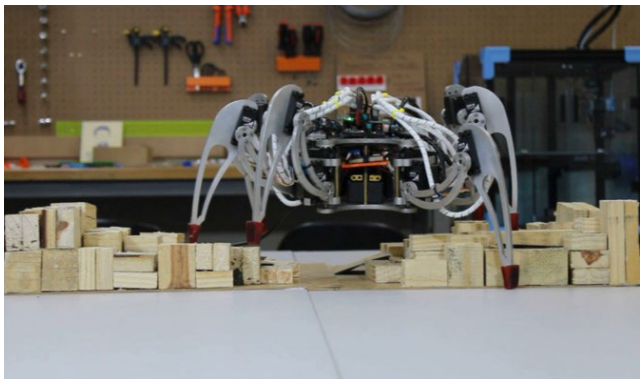

FIGURE 1. The first generation of hexapod robots developed at the Applied Control Laboratory. Biologically Inspired Hexapod Robot named Myrmex.

describes the complete kinematic model for solving these two systems. The robot parameters are described in Appendix A and the detailed procedure of this model are presented in Appendix B.

The concept of generalized coordinates was used to represent the motion of floating base systems. The Myrmex hexapod robot, presented in Figure 1, has 24 DoF, including 6 unactuated DoF that specify the Cartesian position and the body orientation represented by the vector

$$q_b = \begin{bmatrix} x_b & y_b & z_b & \alpha & \beta & \varphi \end{bmatrix}^\top, \tag{1}$$

where x_b, y_b and z_b represent the Cartesian position, α, β and φ represent the orientation of a coordinate system attached locally to the robot base, and measured with respect to some fixed world coordinate system. The remaining 18 DoFs correspond to the actuated joint angles of each leg, here defined as

$$q_a = \begin{bmatrix} q_{11} & q_{21} & \dots & q_{ji} \end{bmatrix}^\top, \tag{2}$$

being q_{ji} the joint angle j of the i-th leg, with $i \in \{1, 2, 3, 4, 5, 6\}$ and $j \in \{1, 2, 3\}$.

The complete configuration of a rigid-body robot with a floating base can be represented by the vector $q = \begin{bmatrix} q_a^\top & q_b^\top \end{bmatrix}^\top \in \mathbb{R}^{24}$. As represented in Figure 2, the system $\{B\}$ is rigidly fixed to the robot's floating base, which can be arbitrarily displaced with respect to the global system $\{G\}$.

A. INVERTED KINEMATICS OF THE LEGS

This section describes the inverse kinematic solution for individual legs. Initially, variables were described in the task space in relation to the system $\{B\}$. When considering each leg separately as an individual manipulator, we use the relation ${}^B\mathbf{T}_{L_i} \in \mathbb{R}^{4\times4}$ to represent the homogeneous transformation between the coordinate systems $\{B\}$ and $\{L_i\}$, such that

$${}^B\mathbf{T}_{L_i} = \begin{bmatrix} R_i & P_{foot_i} \\ 0 & 1 \end{bmatrix}. \tag{3}$$

In (3), $\mathbf{P}_{foot_i} \in \mathbb{R}^3$, $\mathbf{R}_i \in \mathbb{R}^{3\times3}$ and represent the position and rotation matrix of the support point of the i-th robot leg related to the system $\{B\}$, respectively. Denavit-Hartenberg notation [37], [38] was used to describe the geometry of the legs. Intermediate coordinate systems were systematically assigned to each joint, respecting the significant constraints of each frame in the coordinate system from the base to the support point of the leg.

For each i leg, the single-leg Jacobians are computed. For this, after determining the forward kinematic model of each leg, $\mathbf{P}_{foot_i}$, it is differentiated with the respective actuated joint angles, i.e,

$$\mathbf{J}_{leg_i} = \frac{\partial \mathbf{P}_{foot_i}}{\partial \mathbf{q}_{a_i}}. \tag{4}$$

Thus, the joint velocities corresponding to each leg are given by

$$\dot{\mathbf{q}}_{a_i} = \mathbf{J}_{leg_i}^{-1} \dot{\mathbf{P}}_{foot_i}. \tag{5}$$

It represents the movement of each leg towards the center of the body. This kinematic solution in open chain, and the control of the position of the stance leg is similar to some other works [23], [24], [25]. However, solving (5) does not solve the body orientation problem.

B. INVERTED KINEMATICS OF EULER ANGLES OF THE BODY

Considering the legs that are in contact with the ground (stance legs), the movement of the body can be determined by describing it in relation to the system of each leg $\{L_i\}$ (a model that transforms joint angles $\mathbf{q}_a$ to the body task space $\mathbf{q}_b$). For this, the following assumptions are considered:

1) The position of each leg is determined and known. This assumptions is easily verified, since we know the initial condition of the robot. Positions after the start are considered accurate using the Jacobian of velocities;
2) The legs do not lose contact with the ground (there is no slip between foot and ground);
3) During the transfer phase, leg movement will not be hindered by an obstacle;
4) The mass of the legs is grouped in the body. It is assumed that the center of gravity is at the centroid of the body;
5) The motion is slow enough that no dynamic effects need to be considered.

To determine the movement of the floating base, the move rate control was used, resorting to the Jacobian matrix of the whole body J_b. In general, this matrix accomplishes the linear mapping between joint space $\mathbf{q}_a \in \mathbb{R}^{18}$ and operational space $q_{b_1} = \begin{bmatrix} x_b & y_b & z_b \end{bmatrix}^\top$, thus

$$q_{b_1} = f(q_a). \tag{6}$$

The linear velocity of the robot CoB in the operational space is given by

$$\dot{q}_{b_1} = J_b \dot{q}_a. \tag{7}$$

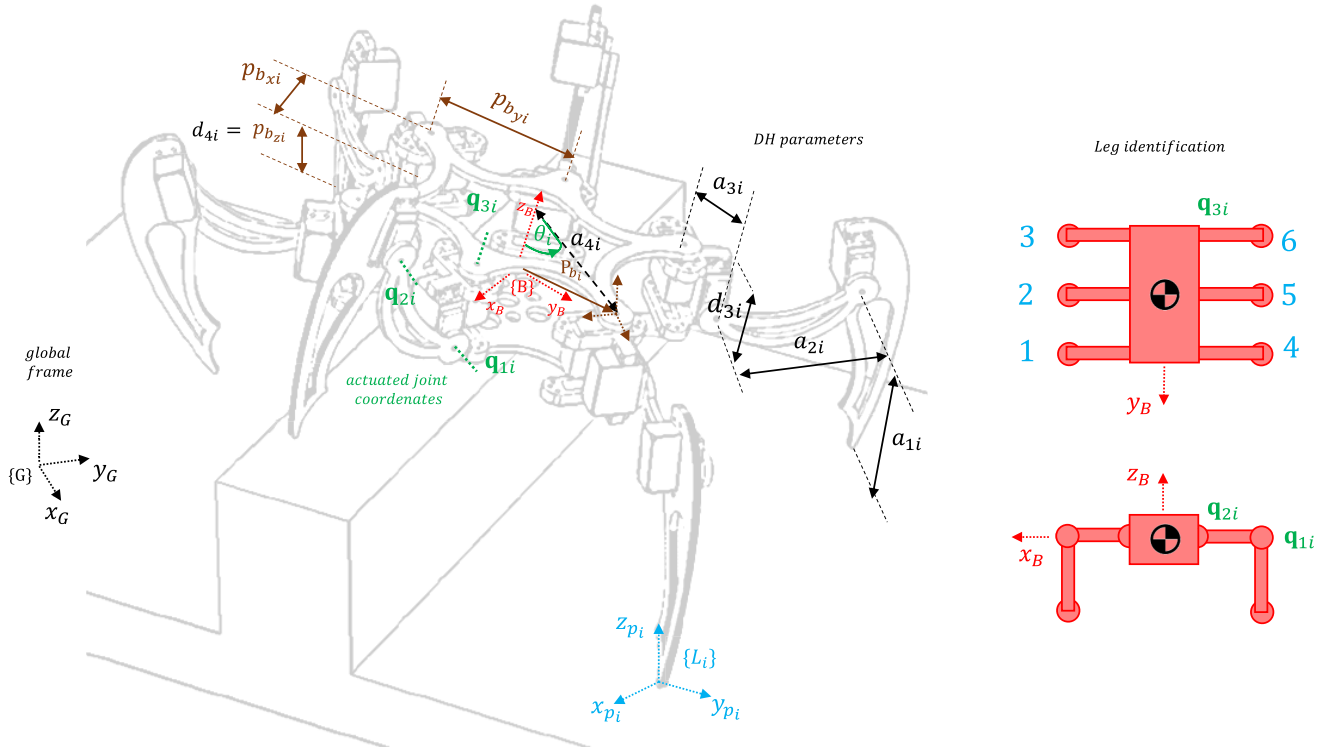

FIGURE 2. Kinematic structure of the Myrmex robot. Floating base system described with actuated and unactuated coordinates system. On the left there are the Denavit-Hartenberg parameters to describe the position and orientation of the support point of the i-th. On the right, the representation of the joint angles j of the i-th leg, with $i \in \{1, 2, 3, 4, 5, 6\}$ and $j \in \{1, 2, 3\}$.

The matrix J_b is determined as

$$J_b = \text{diag}(J_{leg_1}, \ldots, J_{leg_i}) \in \mathbb{R}^{3i \times 3i}. \tag{8}$$

Note that the dimension and values of J_b can be changed at each iteration, based on the positions of q_a, and also on which legs are in the support situation.

Next, it is necessary to determine the kinematics of the body associating the angular velocity of the floating base $\boldsymbol{\omega}_\text{b} \in \mathbb{R}^3$. It is known that the orientation of the support point of the i-th leg is given by $\mathbf{R}_i$ in (3), and it needs to satisfy the rotation matrix $R_\text{b} \in \mathbb{R}^{3\times3}$. The matrix $\mathbf{R}_b$ is based on three successive rotations through the Euler angles, being described in this work as

$$R_\text{b} = R_{z(\varphi)} R_{y(\beta)} R_{x(\alpha)}, \tag{9}$$

where,

$$R_{z(\varphi)} = \begin{bmatrix} \cos(\varphi) & -\sin(\varphi) & 0 \\ \sin(\varphi) & \cos(\varphi) & 0 \\ 0 & 0 & 1 \end{bmatrix}, \tag{10}$$

$$R_{y(\beta)} = \begin{bmatrix} \cos(\beta) & 0 & \sin(\beta) \\ 0 & 1 & 0 \\ -\sin(\beta) & 0 & \cos(\beta) \end{bmatrix}, \tag{11}$$

$$R_{x(\alpha)} = \begin{bmatrix} 1 & 0 & 0 \\ 0 & \cos(\alpha) & -\sin(\alpha) \\ 0 & \sin(\alpha) & \cos(\alpha) \end{bmatrix}. \tag{12}$$

In this way, the rotation speed in relation to the fixed coordinate system at the center of the robot is determined by the antisymmetric velocity matrix

$$\dot{R}_\text{b} R_\text{b}^{-1} = \begin{bmatrix} 0 & -\omega_z & \omega_y \\ \omega_z & 0 & -\omega_x \\ -\omega_y & \omega_x & 0 \end{bmatrix}, \tag{13}$$

hence, it is possible to obtain the angular velocity vector $\boldsymbol{\omega}_\text{b} = \begin{bmatrix} \omega_x & \omega_y & \omega_z \end{bmatrix}^\top$.

The matrix $J_{x_2} \in \mathbb{R}^{6\times6}$ is defined to relate the angular velocities of the body to the angular velocities of the Euler angles, such that

$$J_{x_2} = \begin{bmatrix} I & 0 \\ 0 & \dfrac{\partial \omega_\text{b}}{\partial \dot{q}_{b_2}} \end{bmatrix}, \tag{14}$$

being $q_{b_2} = \begin{bmatrix} \alpha & \beta & \varphi \end{bmatrix}^\top$.

Next, the velocity of the thigh of each leg is determined. Considering the vector that describes the position of the i-th thigh in relation to the center of the body (defined as P_{bi}, as shown in Figure 2), it follows that

$$v_{Pi} = \dot{q}_{b_1} + \boldsymbol{\omega}_\text{b} \times (R_\text{b} P_{bi}), \tag{15}$$

that can be rewritten as

$$v_{Pi} = \dot{q}_{b_1} + \Omega_{leg_i} \boldsymbol{\omega}_\text{b}. \tag{16}$$

being

$$\mathbf{\Omega}_{leg_i} = \begin{bmatrix} 0 & -\lambda_{leg_{zi}} & \lambda_{leg_{yi}} \\ \lambda_{leg_{zi}} & 0 & -\lambda_{leg_{xi}} \\ -\lambda_{leg_{yi}} & \lambda_{leg_{xi}} & 0 \end{bmatrix}, \quad (17)$$

where $\dot{q}_{b_1} = \begin{bmatrix} \dot{x}_b & \dot{y}_b & \dot{z}_b \end{bmatrix}^\top$ corresponds to the translational velocities of the system body $\{B\}$ and $\lambda_{leg_i} = R_b P_{bi} \in \mathbb{R}^{3\times 1}$.

Thus, the following matrix is then defined

$$J_{x_{1i}} = \begin{bmatrix} I & \mathbf{\Omega}_{leg_1} \end{bmatrix} \in \mathbb{R}^{3\times 6}. \quad (18)$$

The matrix $J_{x_{1i}}$ relates the angular velocities of the body to the velocities of the joints of leg i. We stress that this matrix depends on the amount of stance legs. In our application, the Equation (18) considers all the six legs as support. If this number changes, one can simply remove the corresponding $\mathbf{\Omega}_{leg_i}$ line. In the product of the Equations (18) and (14), it follows for any i-th leg i that

$$v_{Pi} = J_{x_{1i}} J_{x_2} \dot{q}_b, \quad (19)$$

$$v_{Pi} = -\dot{\mathbf{P}}_{foot_i}. \quad (20)$$

Hence, assuming that all legs are in the support situation, it follows that

$$-J_b \dot{q}_a = \begin{bmatrix} I & \mathbf{\Omega}_{leg_1} \\ \vdots & \vdots \\ I & \mathbf{\Omega}_{leg_i} \end{bmatrix} J_{x_2} \dot{q}_b, \quad (21)$$

which results in an equation that defines the velocities of the variables of the joint $\dot{q}_a$ in relation to the desired linear and angular velocities of the body $\dot{q}_b$, in the form

$$\dot{q}_a = -J_b^{-1} J_{x_1} J_{x_2} \begin{bmatrix} \dot{x}_b \\ \dot{y}_b \\ \dot{z}_b \\ \dot{\alpha} \\ \dot{\beta} \\ \dot{\varphi} \end{bmatrix} \in \mathbb{R}^{3i\times 1}. \quad (22)$$

III. MYRMEX HEXAPOD ROBOT

In order to validate the developed methodology, experimental results are presented with the robot. Myrmex represents the first generation of hexapod robots developed at the Applied Control Laboratory - LCA - IFSP, Brazil. The current weight of the robot is approximately 3.6 kg, with the weight of each individual component provided in Table 1. Its body is 200 mm long and 105 mm wide. The zero-angle configuration of the robot with the Denavit-Hartenberg notation may differ from the zero-angle configuration set by the joint controller. In such cases, joint angle offsets need to be introduced to achieve the desired zero-angle pose. We have implemented the method [38] that incorporates the required joint angle offsets to achieve the desired zero-angle pose. The configuration of joint controller was chosen, assuming that the legs are fully extended, and in this situation, the legs have a maximum length of 275 mm.

The robot is powered by eighteen HSR 5990-TG servomotors that do not have torque control. These servomotors

TABLE 1. Hardware specification of Myrmex hexapod robot.

Component	Value [kg]	Quantity
Drive Battery	0.312	01
Electronic Battery	0.075	02
Servomotors	0.068	18
Upper Base	0.125	01
Bottom Base	0.130	01
Thigh	0.024	12
Femur	0.032	12
Tibia	0.046	06
Control Board	0.160	-
Sensor Board	0.170	-
Cables and Others	0.300	-
Total Weight	3604	-

communicate with each other through a half-duplex serial line with a data channel speed of 19200 baud and provide the angular position of the joints. The robot's locomotion speed is limited by the number of actuators and the bandwidth of the communication channel between the control board and the servomotors. The serial communication channel has a latency of 72 ms for complete actuation in $\dot{q}_a$. To address this issue, a control system based on an ARM Cortex-M7 at 600 MHz was selected for this research. The system utilizes a Finite State Machine (FSM) to manage information ensuring smooth transitions between the individual controllers of the legs, including the primary and the secondaries (ARM Cortex-M4 at 72 MHz). In the following phases, we will index the elements by the following set:

$$W_{primary} := \{\text{RPL, WBK, LTP, WTL, WSL}\}, \quad (23)$$

$$W_{secondary} := \{\text{RL, WL}\}. \quad (24)$$

The design process of the FSM begins by distinguishing the types of states to legs (support phase or transfer phase). In this work, the force sensors were used solely as contact switches. The decision to transition from one phase to another is based on the position feedback values of the servomotors. Thus, we have the following states: Read Position Leg Phase (RPL), Whole-Body Kinematics Phase (WBK), Leg Trajectory Phase (LTP), Write Transfer Leg Phase (WTL), Write Support Leg Phase (WSL), Read Leg Phase (RL), and Write Leg Phase (WL).

The floating base pose data were estimated by integrating data from a low-cost IMU MEMS (9 DoF) coupled close to the center of gravity and aligned with the main axes of the base. Each sensor is equipped with a 3-axis accelerometer (ADXL345), a 3-axis gyroscope (ITG-3200), and a 3-axis magnetometer (HMC5883L). We developed custom software to acquire 9-axis data. The outputs of all sensors are sampled at 100 Hz and processed by an on-board ATmega328 are illustrated in Figure 3.

IV. FLEXIBILITY AND MOBILITY IN LEGGED ROBOTS

In legged robotics, flexibility and mobility are vital in designing and developing robots capable of efficient and adaptive movement. Although related, these two concepts

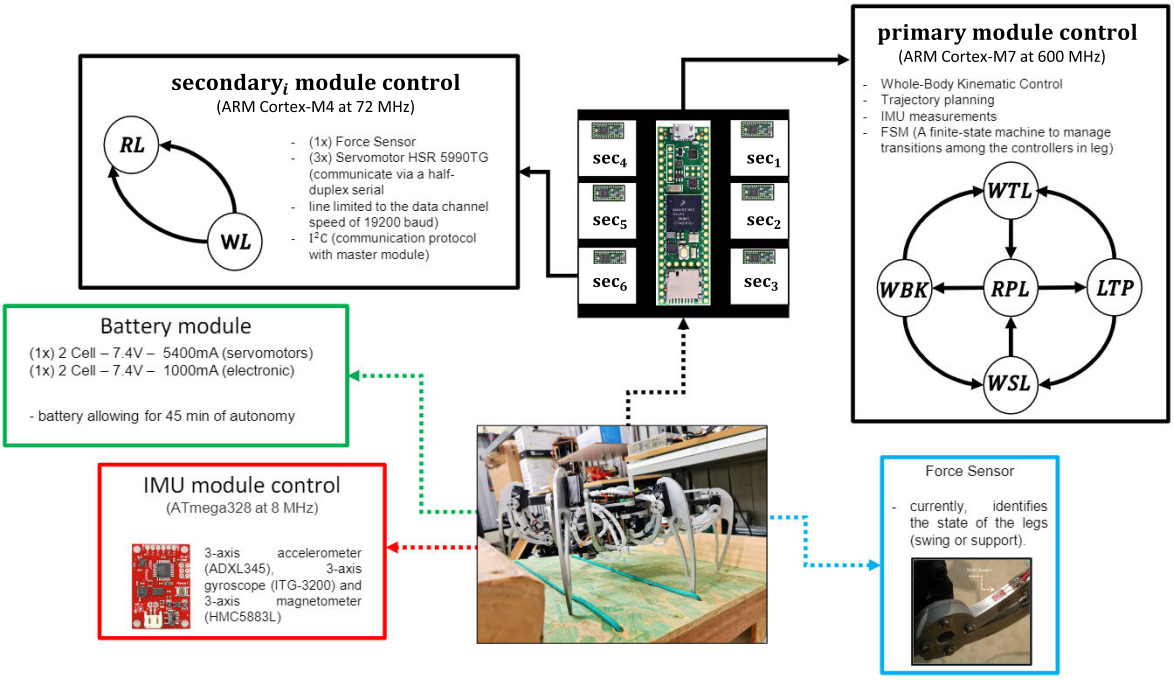

FIGURE 3. Main hardware components of Myrmex and their connectivity. Primary Module Control: A finite-state machine to manage transitions among the controllers in legs. Secondary Module Control: A finite-state machine to manage transitions among the motors (angular position and state) in leg.

have distinct meanings when applied to robots with multiple legs.

A. LEG KINEMATIC FLEXIBILITY

Leg kinematic flexibility is essential for achieving omnidirectional mobility over rugged terrains. It is directly related to proper leg morphology (i.e, default kinematic configuration of a leg). Although the morphological design of the legs is beyond the scope of this research, mechanical coupling and simplicity can be advantageous for flexibility. However, it is important to consider that there is a compromise in mobility. For example, RHex [26], [27] is unable to vary the placement of its feet relative to the body to reach obstacles in a variable manner or search for footholds. So far, several studies have been conducted to investigate the potential impacts of leg morphology in legged robotics. These studies have explored various aspects such as the use of elastic joints [39], inelastic joints [36], flexible leg [40], rigid legs [25], [30] and the ability to perform movements with different ranges of motion using serial legs [41], parallel leg [42], springs [43] or linear actuators [44]. Whether concentrated at the joints or distributed along the ligaments, leg kinematic flexibility has a notable influence on the maximum stride length, maximum obstacle height that the robot can overcome, and the ability to position and orient the foot tips during movement. Additionally, flexibility allows the robot to manipulate objects using some of its legs [30], [45], leveraging the system's redundancy.

The first version of Myrmex was designed to overcome obstacles with a maximum height of 80 mm and a maximum stride length of 100 mm. We adopted rigid legs made of aluminum, resulting in a serial and highly modular structure for easy maintenance. The legs have a non-elastic joint axis that directly actuates the limb to be moved: thigh, femur, and tibia. As will be presented in the Section V, Myrmex is capable of flexibly coordinating its limbs to adapt to various locomotion conditions, such as typical gait patterns, obtaining stable footholds in uneven environments.

B. BODY KINEMATIC FLEXIBILITY

The robot's body flexibility plays a crucial role as a floating base to which the legs in the swing phase are attached. The kinematic flexibility of the body allows for adjusting its position and orientation. This flexibility is significant in challenging terrains with limited footholds, as it enables the legs to reach further and potentially more effectively footholds [46].

In this application, equation (22) allows for the control of movements of the floating base (depending on which legs are fixed to the substrate). As seen in the Section V, the model allows for adjusting the position and orientation of the body to expand the kinematic task space. The vector q_b corresponds to the position and orientation of the Center of Body (CoB) with respect to the global system $\{G\}$.

C. MOBILITY

Mobility refers to the overall ability of the robot to move freely and with control in different directions and planes of motion. The mobility of animals is typically superior to current legged robots. Just like animals, legged robots need

to swerve, dodge, dive, climb, turn, and stop abruptly. A task that requires collaboration between body and leg movements and encompasses not only the flexibility of the legs and body but also stability in legged locomotion. Researchers often employ stability margins to keep the robot away from the stability limit [47], [48], [49], [50], [51]. However, the definition of stability can vary widely. The simplest stability margins are based on the robot's static configuration, where if the projection of the center of gravity (CoG) onto the ground is outside the support polygon, it indicates an uncompensated moment on the foot resulting in rotation along its edge. Traditionally, stability in legged locomotion is taken to refer to stability margin S_M and longitudinal stability margin S_L [50]. The stability margin is the shortest distance S_i from the vertical projection of the CoG to the boundaries of the support pattern in the horizontal plane. The longitudinal stability margin is the shortest distance S_{l_i} from the vertical projection of the center of gravity to the front and rear boundaries of the support pattern. Refer to Figure 4, which illustrates these concepts. An improved stability measure was proposed by Messuri et al. [52]. He defined the Energy Stability Margin (S_{ESM}) as the minimum potential energy required to cause the robot to topple around the edges of the support polygon. Finally, Hirose et al. [51] normalized S_{NESM} to the robot weight and proposed the Normalized Energy Stability Margin (S_{NESM}), defined as that is:

$$S_{NESM} = \min_{i}^{n_{sp}}(h_i), \tag{25}$$

where i represents the segment of the support polygon that is considered the rotation axis, n_{sp} is the number of supporting legs, and h_i represents the variation in CoG height during the tumble, given by

$$h_i = |\mathbf{R_i}|\,(1 - \cos\alpha)\cos\beta. \tag{26}$$

In equation (26), $\mathbf{R_i}$ is the distance from the CoG to the rotation axis, α is the angle that $\mathbf{R_i}$ forms with the vertical plane, and β is the inclination angle of the rotation axis relative to the horizontal plane. The S_{NESM} has been identified as the most effective stability margin for statically stable gait [53]. However, when walking involves dynamic effects, it becomes challenging to accurately assess machine stability. It is important to note that this topic falls outside the scope of this research, and for further knowledge, the reader is encouraged to refer to [54].

In this research, the minimum requirement to attain stability margin is a tripod of support. If a robot's CoG falls outside the pattern of support formed by its feet on the ground, it is statically unstable and will fall. The desired motion of the floating base involves the legs in the stance phase, and the desired motion of the swing legs does not contribute to body stabilization (see Figure 5).

In the Section VI, we present the mobility of the Myrmex robot walking on irregular surfaces. The robot's stability during operation in challenging terrains relies solely on proprioceptive information rather than explicit terrain data.

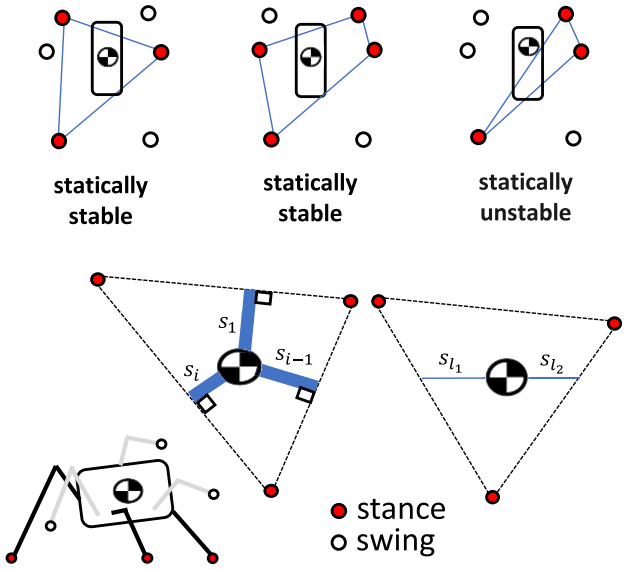

FIGURE 4. Gait Planning. Free walking movements are achieved through a combination of closed and open kinematic chain. The representation of the joint angles j of the i-th leg, with $i \in \{1, 2, 3, 4, 5, 6\}$ and $j \in \{1, 2, 3\}$.

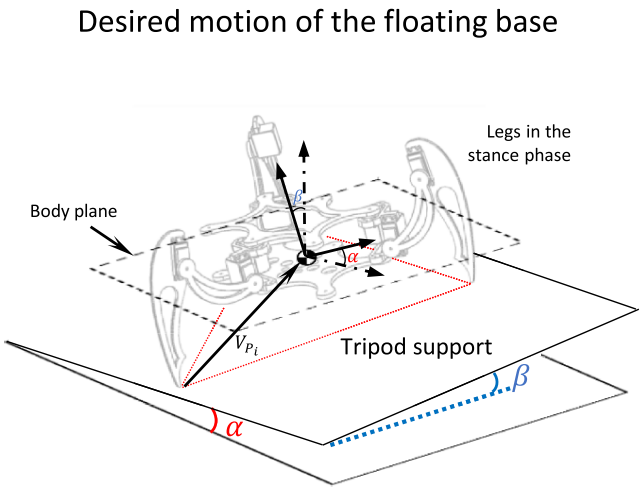

FIGURE 5. Desired motion of the floating base. The movement involves the legs in the stance phase, and the desired motion of the swing legs does not contribute to body stabilization.

By considering whole-body kinematics, the controller can adjust the robot's center of gravity and posture to improve stability.

V. EXPERIMENTAL VALIDATION - STATIC SITUATIONS

The first set of experiments explores the robot's whole-body model to enhance its flexibility in the task space. Body posture is considered to reach locations that would be kinematically challenging for leg control alone.

A. LEG FLEXIBILITY

To validate the model in flexible situations, we propose six experimental scenarios that cover translation and rotation cases. We define a standard displacement of 1 mm applied in

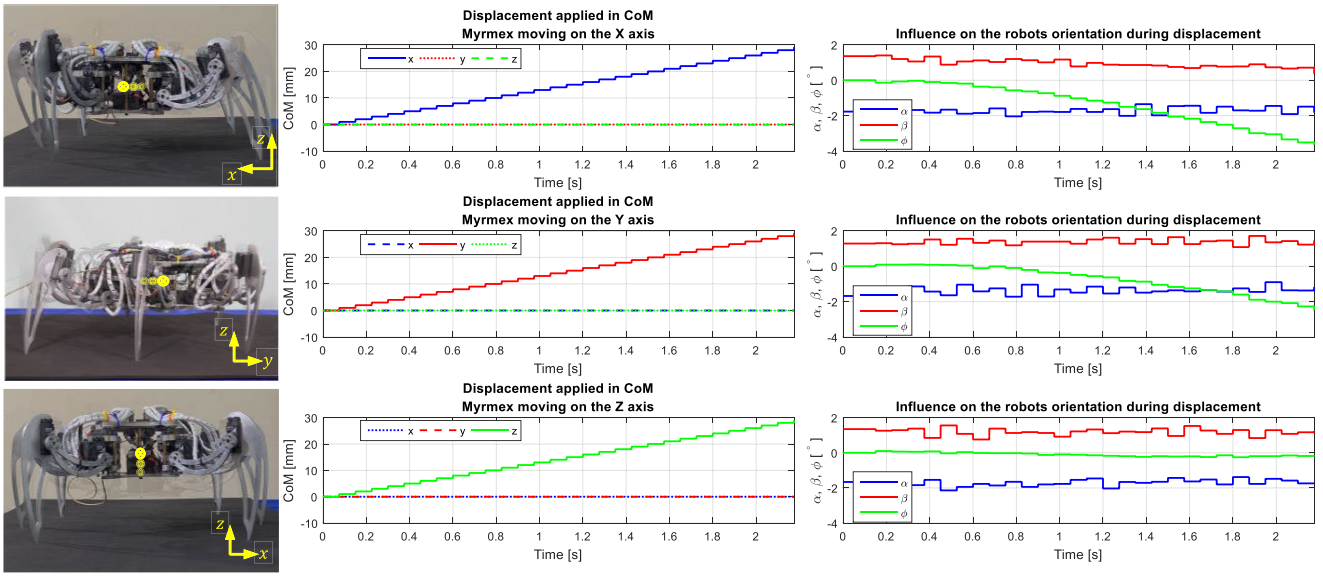

FIGURE 6. Initial and final movement of model validation, considering body translation. From left to right, it consists of translations on the x, y and z axes, respectively. Result considering body translation. Speed of approximately $v_i = 0.0133$ m/s (1 mm for each interaction with $T_s = 75$ ms).

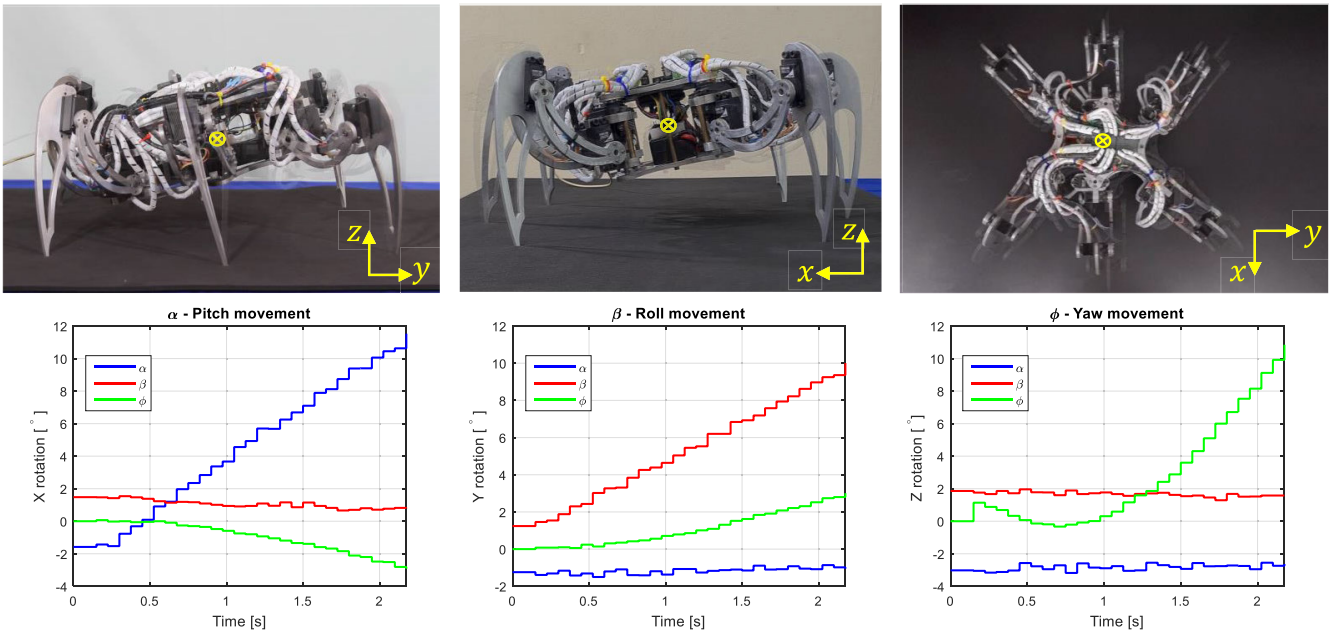

FIGURE 7. Initial and final movement of model validation, considering body rotation. From left to right, it consists of rotations on the x, y and z axes, respectively. Result considering body rotation. The desired angular velocity in each case is equal to $\omega_i = 0.0133°/s$ (1° for each interaction with $T_s = 75$ ms).

the x, y, and z directions within a specific time interval $T_s = 75$ ms. These values are individually used in the $\dot{q}_b$ vector while keeping the other elements as zero.

The remaining three experiments validate the model for the angles α, β, and φ, which represent the orientation of a coordinate system attached locally to the robot base and measured with respect to the fixed global coordinate system. Similarly, we propose individual displacements of 1° around each axis.

The obtained results are presented in two groups: **Group A** focuses on the translational motion of the robot's center of gravity, while **Group B** analyzes the rotational movement around the coordinate system fixed to the CoB.

The Figure 6 illustrates the translational motion and the corresponding results for the cases in **Group A**. In each case, a velocity of approximately $v_b = 0.0133$ m/s was applied. The practical results align with expectations, as the inverse kinematic model accurately computes the joint angles required to achieve the desired motion.

For **Group B**, the rotational motion and the measured results are depicted in Figure 7. In this case, a desired angular velocity of $\omega_b = 0.0133\,°/s$ (equivalent to a rotation of 1° per

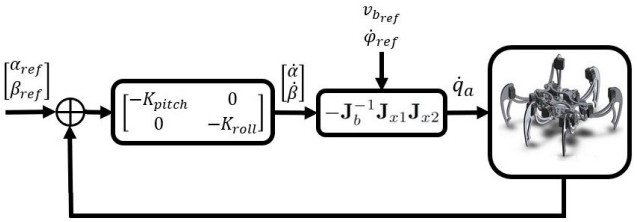

FIGURE 8. Control diagram of pitch (α) and roll (β) angles of the Myrmex.

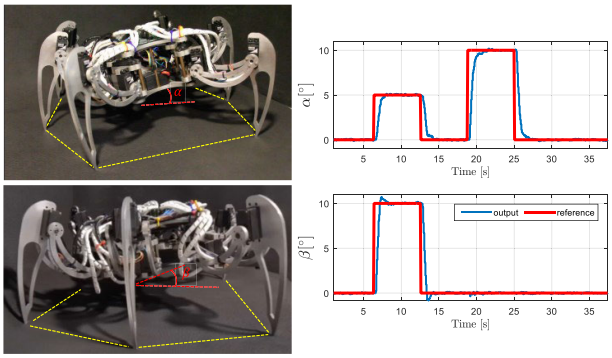

FIGURE 9. Myrmex robot followed a pre-determined trajectory. Reference values were imposed, and the output was measured at all times.

interaction with $T_s = 75$ ms) was considered. Once again, the practical results validate the accuracy of the developed model. It is worth noting that, besides the rotational angle around the axis, other variables may exhibit changes due to noise and trends present in the IMU. However, for our application, these variations were small (approximately 2°), and the overall results were satisfactory.

These results validate the accuracy of the developed model, demonstrating its effectiveness in predicting and controlling the robot's movements.

B. ATTITUDE CONTROL - BODY FLEXIBILITY

It is desirable to maintain the position of the center of gravity on the specified trajectory. When the CoG is elevated above the ground, it is crucial to ensure the stability (static or dynamic) of the body's tilt and rotation to maintain balance.

Considering the whole-body kinematic model, a controller was proposed for the floating base orientation (see Figure 8). Experiments were conducted to enable the robot to adapt its body posture according to the terrain inclination. A test platform with a MEMS IMU attached to its center was used to introduce disturbances in the control system. The platform inclinations were measured at the same sampling frequency as the control loop.

The robot's joint angles obtained from its IMU and the body's reference velocity were utilized. Based on the kinematic model, the body's position and orientation are controlled solely through the leg motions in the support phase. A control system was designed to take posture error as input and the joint velocities of each leg during the support phase as output. It is important to note that in each interaction, the control calculates a desired velocity that is applied to the model. In the next interaction, a new velocity is calculated, thus maintaining consistent control operation time with the transition algorithm described earlier.

To illustrate the operation of the proposed control, we experimentally conducted four trials considering gains of $K_{pitch} = 0.25$ and $K_{roll} = 0.5$ (the controller gains were adjusted experimentally).

1) **Following a trajectory**: In the first trial, the robot followed a pre-determined trajectory. Reference values were imposed, and the output was measured at all times. Results are presented in Figure 9. It can be observed that the control had satisfactory performance in the trajectory following problem. The proposed control determines the angular velocity of each variable, and then, using the inverse kinematic model of the whole body, the motion of each motor is performed.
2) **Posture control (six legs)**: In the second trial, the Myrmex was placed on a test platform where it could be disturbed by increasing or decreasing the tilt and rotation angles. During the test, the references were set to zero ($\alpha = 0$ and $\beta = 0$), while the platform was perturbed. Results are illustrated in Figure 10(a). The test platform simulates an uneven terrain that causes undesired tilting and rotation movements. The control performed as expected, and the Myrmex was able to maintain the body orientation at 0°, even when the test platform applied a disturbance of ±20°. A small oscillation is observed, mainly in β, but this oscillation is negligible compared to the magnitude of the disturbance.
3) **Posture control (three legs)**: The third trial was similar to case 2, but only three legs were in contact with the ground (legs 1, 3, and 5). This configuration validated the model for situations with only one tripod of support to achieve static stability. Figure 10(b) shows the results and similar to case with six legs in the support phase. The robot was able to reject with satisfactory performance.
4) **Unevenness between the legs**: Finally, a test of unevenness between the legs is conducted. The robot is placed on a table with platforms that can be individually inserted or removed for each leg, altering the leg height. The purpose of this experiment is to determine whether Myrmex is capable of adjusting its parameters according to the terrain topology and simulate conditions such as loose rocks or scattered debris during robot operation. The results obtained are presented in Figure 11. In this case, the green lines (labeled as d_i) represent disturbances applied to the legs, as follows: d_1 - Insertion of a platform in leg 2, d_2 - Insertion of a platform in leg 3, d_3 - Insertion of a platform in leg 1, d_4 - Insertion of a platform in leg 4, d_5 - Removal of the platform in leg 4, d_6 - Insertion of a platform in leg 6, and d_7 - Removal of the platform in leg 6. The robot has no prior information about the location or magnitude of the height changes. It is able to respond to unexpected alterations on the surface, correcting its body posture in the presence of unexpected disturbances in its legs.

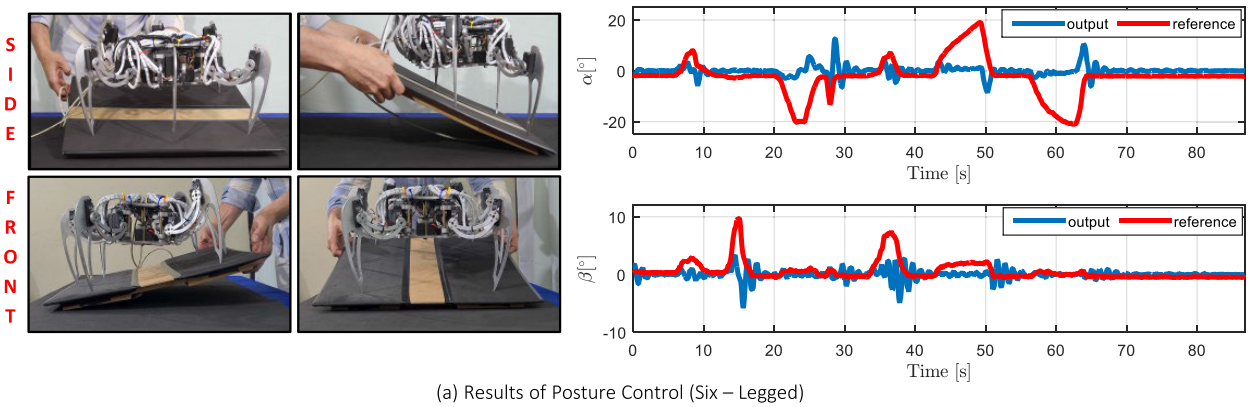

(a) Results of Posture Control (Six – Legged)

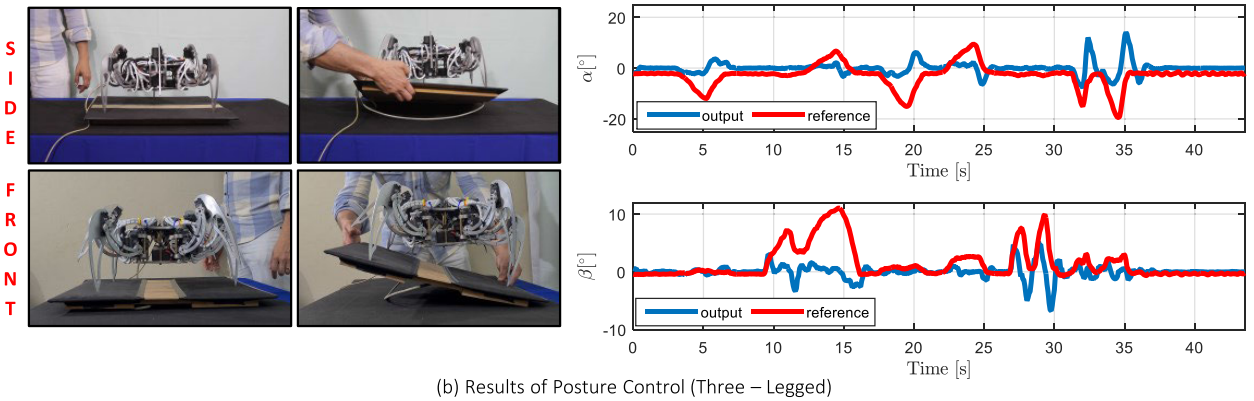

(b) Results of Posture Control (Three – Legged)

FIGURE 10. Experiment with six and three legs in the stance phase. Side views are presented in the upper row, and front views are shown in the lower row. Results of Case B (six legs in stance phase). Adaptive behavior of the robot body to handle high slope gradients. Disturbances of ±20° in α and ±10° in β are applied by the test platform. Results of Case C (three legs in stance phase). Adaptive behavior of the robot body to handle high slope gradients. Disturbances of ±20° in α and ±10° in β are applied by the test table.

As shown in Figure 11, the controller successfully rejects the perturbations in all cases, maintaining the desired values of α_{ref} and β_{ref}.

In all experiments, the Myrmex robot had no information about the environment, and no external sensors were used. The CoB position is adjusted to increase the stability margin [53] in inclined terrain situations. The joint angles are adjusted to align the foot tip parallel to the gravity vector. Previous research [23] has shown that this postural control enhances energy efficiency and maneuverability by reducing the effort required to support gravitational forces. This approach has improved performance in climbing steep slopes and reduced the joint torques, as demonstrated in [30], [31], and [55].

VI. EXPERIMENTAL VALIDATION - MOBILITY

In the second set of experiments, evaluates the ability of Myrmex to walk on uneven terrain. The chosen geometric features for this study includes gradients and steps that are compatible with the dimensions of the robot.

A. GAIT PATTERN

During locomotion when the projection of the COG exits the support polygon, there are two methods to bring it back: accelerating the center of gravity towards the support polygon by modifying the angular momentum, or adjusting the support polygon by taking a step. This allows for control over the trajectory of the robot's center of gravity, ensuring a desired level of stability.

Studies were conducted [56] to examine the static stability margin in all possible regular gaits with six legs. Findings showed that the stability margin is maximized by a regular and symmetric gait defined with $\frac{1}{2} \leq \beta_{leg} < 1$. Being β_{leg} is the duty factor, the fraction of a stride period that a leg is in the support phase [49].

To quantify stability during locomotion, we use not only the support polygon as a reference but also an idealized and simplified version of gait, with alternating and non-overlapping tripods. This means that exactly three legs support the body at any given time. For this purpose, in an alternating tripod gait, the leg selection factor was $\beta_{leg} = 0.5$. Thus, the minimum number of legs was maintained to evaluate the proposed controller.

For the definition of locomotion (see in Figure 12), a desired trajectory was established for i-th leg and the Cartesian coordinates are given by $\mathbf{P}_{traj_i} \in \mathbb{R}^{3\times n_s}$. We predefined the maximum number of points n_s that each leg can receive in order to generate the corresponding joint trajectories $\dot{\mathbf{q}}_{a_i}$. The

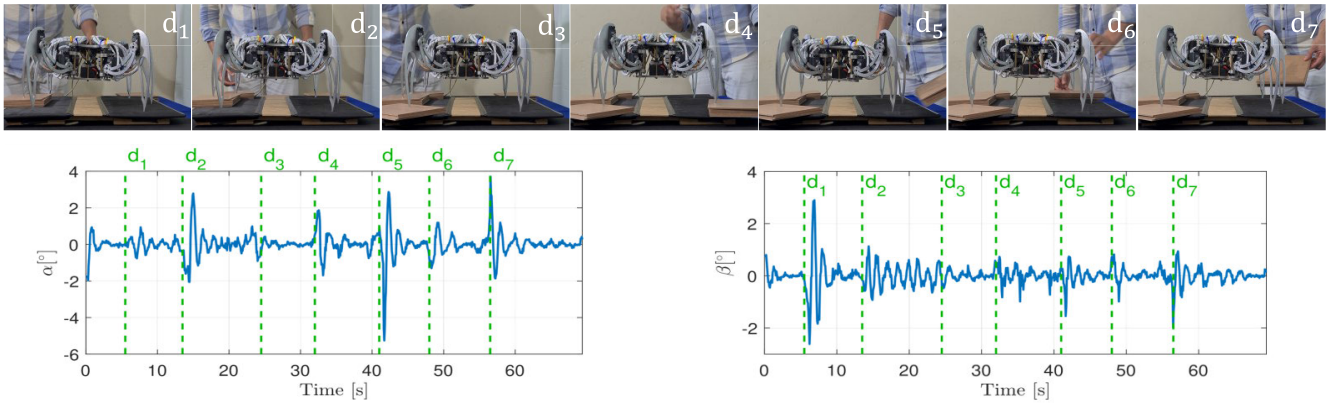

FIGURE 11. Experiment with leg disturbances during the stance phase. Results of case Unevenness between the legs applied during stance phase. Adaptive behavior of the robot body in situations of insertion and removal of a base with different heights.

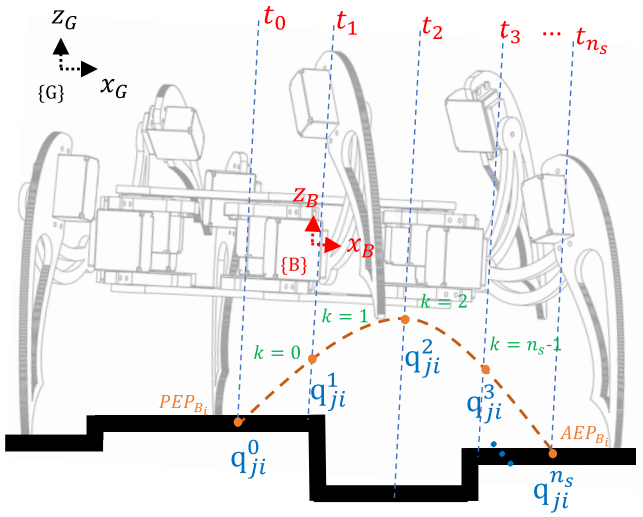

FIGURE 12. Gait Planning. Free walking movements are achieved through a combination of closed and open kinematic chain. The representation of the joint angles j of the i-th leg, with $i \in \{1, 2, 3, 4, 5, 6\}$ and $j \in \{1, 2, 3\}$.

time cycle of leg T_c was divided into two functional states

$$T_c = T_{sp} + T_{tp}. \tag{27}$$

where T_{sp} and T_{tp} are support period and swing period respectively. The duty factor β_{leg} is determined by

$$\beta_{leg} = \frac{T_{tp}}{T_c}. \tag{28}$$

The trajectory guides the leg from its initial point - Posterior Extreme Position (PEP_{B_i}), to its final point, Anterior Extreme Position (AEP_{B_i}). It is important to note that this trajectory does not account for any potential obstacles that may obstruct the leg's path (see Figure 12). The trajectory of the foot should be a continuous and smooth closed curve, with no sudden change in speed and acceleration. After defining the corresponding trajectories, the vector containing kinematically feasible solutions for the joint angles of each leg can be specified as $\mathbf{q}^{n_s}_{ji}$. Again notice that the subscripts j and i are used to represent the joints and legs of the robot, respectively. Therefore, $j = 1, 2, 3$ and $i = 1, 2, 3, 4, 5, 6$. At the beginning of the movement, the primary module control calculates the polynomial that connects the current state and the desired states of the joints in this vector. After the trajectory planning carried out in this first level, considering constraints and zero velocity conditions at the beginning and end of the trajectory, the second level (secondary module control) comes into action, which solely focuses on executing the movement for a given specified locomotion pattern.

B. LOCOMOTION IN IRREGULAR TERRAIN

As the variety of irregular terrains is unlimited, it is challenging to cover all the different cases of walking on uneven terrain. In our research, to facilitate data analysis and validate the model in dynamic scenarios, we set the references for the robot's body posture (pitch and roll angles) to zero to adjust its posture according to the terrain topology. In practice, robots do not simply ascend or descend along a single maximum gradient line. Instead, the center of gravity experiences displacements in both longitudinal and lateral directions. The robot maintained a steady speed of approximately $v_b = 0.06$ m/s during the experiments. Myrmex was configured to walk using a continuous gait in the following terrain scenarios:

1) **Experiment-A**: Irregular terrain with inertial effects (walking on two gradients). This involves traversing vertical steps that form gradients. The body posture needs to be adjusted by compressing the legs on both sides of the robot;
2) **Experiment-B**: Irregular terrain with inertial effects (walking on vertical steps with arbitrary directions). In situations involving ascent and descent formed by steps, the robot's posture needs to be adjusted accordingly with reference;
3) **Experiment-C**: Horizontal and flat terrain with inertial effects (walking on vertical steps with a gradient).

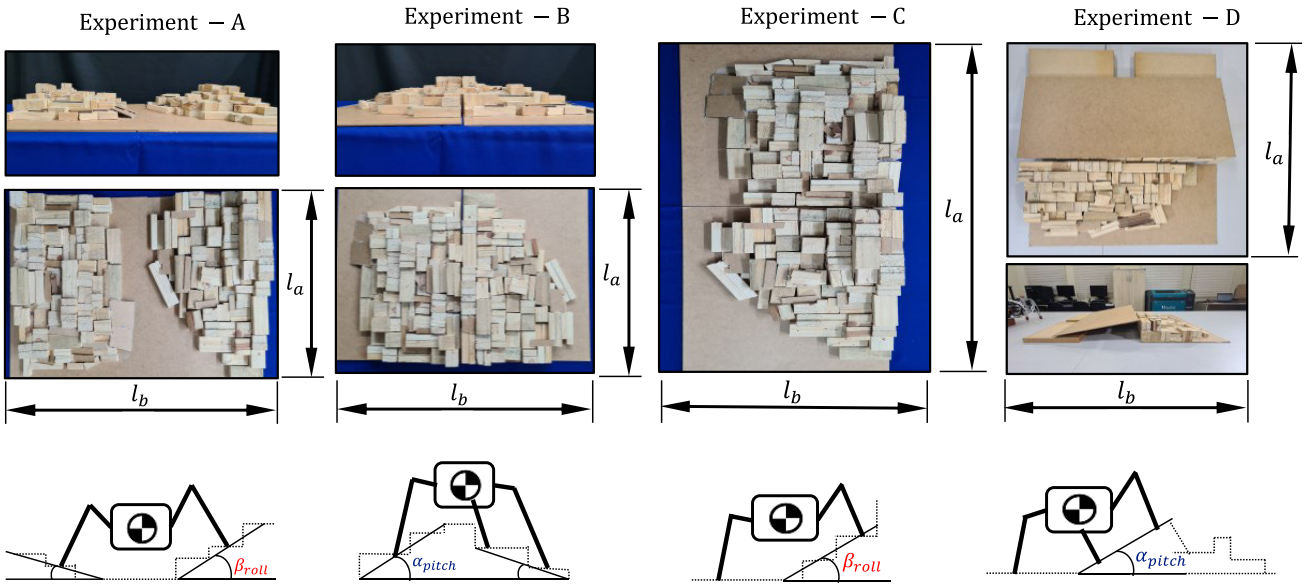

FIGURE 13. Dynamic scenarios - experiments that induced displacements of the CoG in the longitudinal and lateral directions. From left to right we have: Experiment-A (walking on two gradients), Experiment-B (walking on vertical steps with arbitrary directions), Experiment-C (walking on vertical steps with a gradient) and Experiment-D (Walking on gradient with lack of substrate contact).

During locomotion, to correct the body posture, the legs on the ascending side will be adducted, while the legs on the flat surface will be abducted;

4) **Experiment-D**: Incline on a flat terrain with inertial effects (walking on gradient with lack of substrate contact). The robot needs to maintain a specified reference during ascent on a flat surface and correct its posture as soon as it loses contact with the substrate.

In order to study this problem the reals terrain features are simplifield into geometric features (abstacles of simple geometry are assumed). Figure 13 shows the geometries of these features. Each can be described by one or two parameters (pitch angle (α_{pitch}), roll angle (β_{roll}) and square blocks height variation of vertical steps δ_{hi}) summarized in Table 2.

It was observed during all experiments that the control readjusts the robot's posture during the support time T_{sp}. Thus, the center of gravity is not shifted if body attitude is kept level. The body can be complete leveling only when the angles of the gradients are smaller than the limiting pitch and roll angles. These limiting angles are determined to be:

$$\alpha_{max} = \tan^{-1} \frac{h_b}{P_{y_i}} \tag{29}$$

$$\beta_{max} = \tan^{-1} \frac{h_b}{P_{x_i}}. \tag{30}$$

where h_b is a given body height. For the Myrmex during the experiment $\alpha_{max} = 23.38°$ and $\beta_{max} = 27.75°$.

The data related to the experiments are presented at the beginning of Figure 14. To ensure body stability while traversing rough terrain, Myrmex initiates its locomotion on a horizontal surface with a pre-specified tripod gait. During

TABLE 2. Geometry of the four experiments.

Experiment	l_a[mm]	l_b[mm]	α_{pitch}[°]	β_{roll}[°]	δ_{hi}[mm]
A	800	1000	±15°	±12°	±15
B	800	1000	±15°	±15°	±20
C	1600	500	±12°	±12°	±15
D	1100	800	±15°	±15°	±45

locomotion, the robot encounters a surface with vertical steps forming two gradients (see Figure 14(A)). Since the robot does not have impedance control nor a camera, the swing legs follow a predefined trajectory in Cartesian space until all the points are reached. The contacts tend to tilt the floating platform to the left or right, as well as inclinations upward and downward. The IMU data illustrate the dynamic behavior during locomotion. Peaks of inclination occur at the moment of leg contact with the terrain. The disturbance generated by contact with the irregular terrain is corrected during the support time. The locomotion control allows the robot to return to its initial reference posture (horizontal surface condition).

In the second experiment (see Figure 14(B)), the robot walked on an irregular surface in an arbitrary direction. The vertical steps formed ascending and descending inclinations throughout the path. The IMU inertial data show this behavior. Note that α angle exhibits negative situations (counterclockwise rotation around the x-axis) during the ascent and positive rotations during the descent.

In the next experiment, as Myrmex initiated each step, the moments of inertia caused by the angular rotation of the robot's body tended to tilt the body to the left (clockwise rotation around the y-axis) and perform an upward tilting movement (clockwise rotation around the x-axis). The IMU

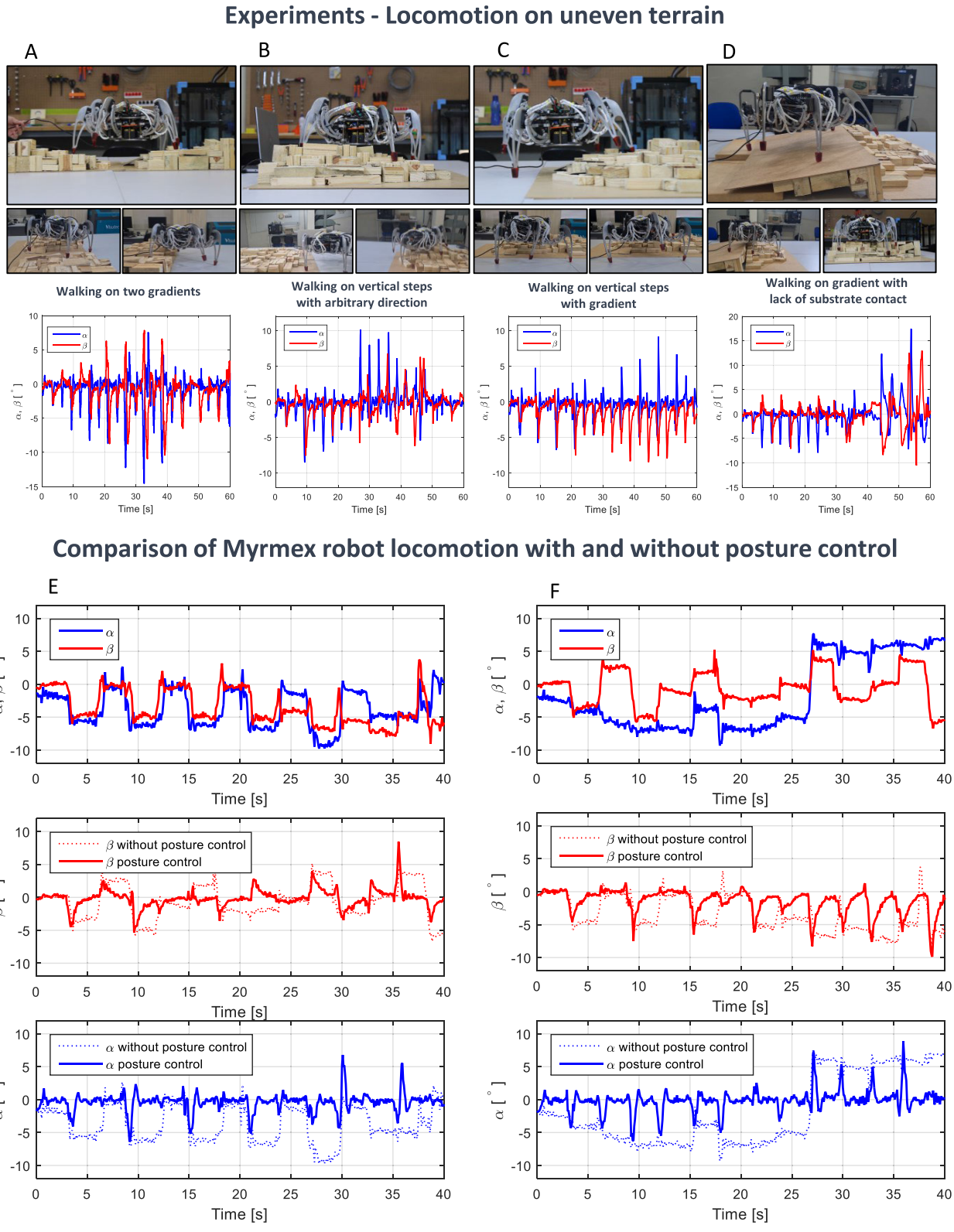

FIGURE 14. Locomotion on uneven terrain. Four experiments aimed at validating the whole body kinematic control in dynamic situations. (A) walking on two gradients, (B) walking on vertical steps with arbitrary directions, (C) walking on vertical steps with a gradient and (D) walking on gradient with lack of substrate contact. Myrmex demonstrated the ability to adjust its posture parameters and CoG position according to the terrain topology. The last two experiments (E) and (F), focus on comparing the effects of the controller action in scenarios with and without body attitude control in scenarios 1 and 2, respectively.

TABLE 3. Locomotion and sensing requirements of hexapod robots.

Author	Robot	Mass [kg]	Actuated DoF [Leg]	Body Posture	Legged Gait Kinematic Chains [open/close]	Proprioceptive Sensor	Exterioceptive Sensor	Impedance Control
Gorner [23]	DLRCrawler	3.5	4	no	open	force, encoder	camera	yes
Belter [24]	Messor II	2.5	3	no	open	IMU, encoder	camera	no
Goldschmidt [25]	Amos II	4.2	3	no	open	contact, encoder	IR, ultrassonic	no
Saranli [26]	RHex	8.2	1	no	open	encoder	no	no
Cheah [29]	Corin	4.6	3	no	open	force, IMU, encoder	no	no
Roennau [30]	Lauron V	40	4	yes	open	IMU, encoder	camera, IR	no
Bjelonic [31]	Weaver	10.3	5	yes	open	IMU, encoder	camera	yes
Zhou [40]	Qingzhui	60	2	no	open	encoder	no	no
Bachega	Myrmex	3.6	3	yes	open and close	IMU, encoder	no	no

data show only negative variations in β (leftward roll inclinations) and positive variations in α (upward body pitch), confirming the proposal of locomotion on a horizontal plane with inertial effects. Figure 14(C) shows that the movements were again decelerated and reversed by the control action.

The last experiment demonstrates how the robot can handle sudden terrain transitions. When a robot faces a slope, it is crucial for it to avoid tipping over. Similar to the previous experiments, throughout the gait, the center of gravity only moves when all three legs are supporting, which increases the stability margin. Additionally, Myrmex maintained its corrected posture while ascending the ramp. When leveling the floating base posture, the rear and front legs were adjusted as the robot climbed the ramp and during disturbances on the uneven terrain. Since the center of gravity moves in relation to the positions of the legs on the ground, and the probability of falling increases as the center of mass approaches the edge of the support triangle, we intentionally directed the robot to cause a fall when crossing a gap in the middle of the course. Once again, the locomotor control action suppressed disturbances to maintain stability on rough terrains. The results are presented in Figure 14(D).

Although during this study, Myrmex exhibited continuous stability in the center of gravity, there were cases where the CoG was outside the polygon formed by the support legs, but the robot did not fall. We refer to this as dynamic stability, where the robot experiences a momentary fall in one direction until new support legs make contact with the ground. Dynamic stability was only observed as the robot does not yet possess dynamic adjustment algorithms to prevent falls, and the swing legs follow a predefined trajectory in Cartesian space. Nevertheless, this can be noticed particularly during scenarios 1 and 2, where there was a lack of substrate contact. During these moments, the CoG shifted forward, but during continuous gait, new contact points occurred, and the proposed model corrected the posture using these points.

Myrmex demonstrated the ability to adjust its posture parameters and CoG position according to the terrain topology. Figures 14(E) and 14(F) present the results of locomotion without posture control in scenarios 1 (walking on two gradients) and 2 (walking on vertical steps with arbitrary directions), respectively. Below each figure, comparisons are shown to assess the effect of control on α_{pitch} and β_{roll} angles. The orientation angles were maintained at approximately $0 \pm 0.35°$ for pitch and $0 \pm 0.55°$ for roll. The video in the following URL shows the experiments: https://www.youtube.com/watch?v=j1W9c7lFOmA.

VII. DISCUSSION

While the Myrmex robot demonstrated the ability to adjust its posture parameters and CoG according to the terrain topology, previous works showed similar performance with some caveats. Locomotion and sensing requirements were summarized in Table 3, in comparison to hexapod robots for which results have been previously reported at similar size scales and actuations as the Myrmex. In the summarized cases, locomotion in hexapod robots occurred using the open chain kinematic model. This method allows robot movement but does not enable control of the body posture. Specific cases, such as the works by Roennau et al. [30] and Bjelonic et al. [31], achieved posture control but at the cost of increasing the degrees of freedom per leg (4 DoF and 5 DoF in the case of Lauron V and Weaver, respectively). This approach increases the number of motors, leading to higher energy consumption and control complexity. Our experiments demonstrated that the Myrmex robot overcame obstacles up to 36.3%, equivalent to 100 mm of its extended leg length and adjusted posture for inclinations up to 20°. The number of DoF significantly affects hexapod robot mobility. However, it cannot be most reduced as seen in the case of the RHex robot [26], with legs having just 1 DoF (without body posture control) or overly redundant, as in the cases mentioned above with 4 DoF or more per leg. Our method showcased robust performance by exploiting hybrid actuation in open and closed kinematic chains with only 3 DoF per leg.

Although there is still room for improvement, we can modify the body height h_b to expand posture parameters (α_{max} and β_{max}). There are other notable limitations. During the leg trajectory in the swing phase, the robot collided with obstacles or encountered a lack of substrate during gait. This caused posture disruptions, which were corrected in real time by the legs during the stance phase. To address collisions, it would be beneficial to add impedance control to enhance collision free locomotion.

VIII. CONCLUSION

This work presented Myrmex, a hexapod robot with 24 DoF, and a whole-body kinematic model was developed that increases the robot's flexibility and mobility. The model considers acting on the position and orientation of the body,

TABLE 4. Kinematic parameters of the legs (Denavit-Hartenberg notation).

Segment	a_{ji}[mm]	γ_{ji}[°]	d_{ji}[mm]	q_{ji}[°]
Body	a_{4i}	0	45	θ_i
Thigh	24.9	γ_{3i}	-60	q_{3i}
Femur	101	0	0	q_{2i}
Tibia	151	0	0	q_{1i}

TABLE 5. Kinematic parameters of the body.

i	1	2	3	4	5	6
θ_i[°]	61.25	0	-61.25	118.75	180	-118.75
$P_{b_{xi}}$[mm]	52.9	65	52.9	-52.9	-65	-52.9
$P_{b_{yi}}$[mm]	96.4	0	96.4	96.4	0	-96.4
$P_{b_{zi}}$[mm]	45	45	45	45	45	45

regardless of the number of legs in contact with the ground. The proposed algorithms deal only with proprioceptive information of the structure. The proposed controller was evaluated in a real robot and practical results were presented.

During all experiments, it was consistently observed that the model actively readjusts the robot's posture using its support legs. As a result, as long as the body maintains a level attitude, the center of gravity remains unchanged. Myrmex demonstrated significant advantages during locomotion on surfaces with gradients, particularly with its hind legs, which facilitated movement on inclined terrains. The robot possesses several desirable characteristics, including the ability to traverse uneven terrain and maintain a stable posture even on steep inclines. Myrmex keeps CoG within the support polygon or adjusts its posture to ensure the CoG remains unaffected. The robot was able to correct its posture on terrain with gradients greater than 20° in any direction relative to the body structure, with only 3 DoF per leg.

The proposed model has been designed for situations where the vision system or exteroceptive sensors of legged robots might fail in adverse environmental conditions. As future work, our goal is to enhance the locomotion performance of the Myrmex robot by integrating whole-body kinematic control with an impedance controller. We will expand the proposed method by controlling the interaction with the environment. The robot's workspace can be explored by seeking more daring body configurations, such as crossing ditches.

APPENDIX A ROBOT PARAMETERS

The mechanical and geometric parameters of Myrmex are defined in Figure 2 and summarized in Table 4 and Table 5. With $\gamma_{3i} = 90°$ for $i \in \{1, 2, 3\}$, and $\gamma_{3i} = -90°$ otherwise, $a_{4i} = \sqrt{{P_{b_{xi}}}^2 + {P_{b_{yi}}}^2}$.

APPENDIX B WHOLE BODY KINEMATIC CONTROL

This Appendix presents the whole body kinematics used for simulation and control purposes. Equation (3) represents the homogeneous transformation between the coordinate systems $\{B\}$ and $\{L_i\}$. The orientation of each leg is represented by

$$R_i = \begin{bmatrix} r_{11_i} & r_{12_i} & r_{13_i} \\ r_{21_i} & r_{22_i} & r_{23_i} \\ r_{31_i} & r_{32_i} & r_{33_i} \end{bmatrix}, \tag{31}$$

with

$$r_{11_i} = c(q_{1i} + q_{2i})c(q_{3i} + \theta_i) \tag{32}$$
$$r_{12_i} = -s(q_{1i} + q_{2i})c(q_{3i} + \theta_i) \tag{33}$$
$$r_{13_i} = s(\gamma_{3i})s(q_{3i} + \theta_i) \tag{34}$$
$$r_{21_i} = c(q_{1i} + q_{2i})s(q_{3i} + \theta_i) \tag{35}$$
$$r_{22_i} = -s(q_{1i} + q_{2i})s(q_{3i} + \theta_i) \tag{36}$$
$$r_{23_i} = -s(\gamma_{3i})c(q_{3i} + \theta_i) \tag{37}$$
$$r_{31_i} = s(\gamma_{3i})s(q_{1i} + q_{2i}) \tag{38}$$
$$r_{32_i} = s(\gamma_{3i})c(q_{1i} + q_{2i}) \tag{39}$$
$$r_{33_i} = 0. \tag{40}$$

The position $P_{foot_i} = \begin{bmatrix} P_{x_i} & P_{y_i} & P_{z_i} \end{bmatrix}^\top$ of leg i is a function of the joint components $\mathbf{q}_{a_i}$, such that

$$P_{x_i} = a_{4i}c(\theta_i) + c(q_{3i} + \theta_i)(a_{3i} + a_{2i}c(q_{2i}) + a_{1i}c(q_{1i} + q_{2i})), \tag{41}$$
$$P_{y_i} = a_{4i}s(\theta_i) + s(q_{3i} + \theta_i)(a_{3i} + a_{2i}c(q_{2i}) + a_{1i}c(q_{1i} + q_{2i})), \tag{42}$$
$$P_{z_i} = d_{4i} + d_{3i} - a_{2i}s(\gamma_{3i})s(q_{2i}) - a_{1i}s(\gamma_{3i})s(q_{1i} + q_{2i})). \tag{43}$$

For the purpose of notation simplification, c and s represent cos and sin, respectively.

The Jacobian matrix of each leg is given as

$$\mathbf{J}_{leg_i} = \begin{bmatrix} j_{11_i} & j_{12_i} & j_{13_i} \\ j_{21_i} & j_{22_i} & j_{23_i} \\ j_{31_i} & j_{32_i} & j_{33_i} \end{bmatrix}, \tag{44}$$

where

$$j_{11_i} = -s(q_{3i} + \theta_i)(a_{3i} + a_{2i}c(q_{2i}) + a_{1i}c(q_{1i} + q_{2i})), \tag{45}$$
$$j_{12_i} = -c(q_{3i} + \theta_i)(a_{2i}s(q_{2i}) + a_{1i}s(q_{1i} + q_{2i})), \tag{46}$$
$$j_{13_i} = -a_{1i}c(q_{3i} + \theta_i)s(q_{1i} + q_{2i}), \tag{47}$$
$$j_{21_i} = c(q_{3i} + \theta_i)(a_{3i} + a_{2i}c(q_{2i}) + a_{1i}c(q_{1i} + q_{2i})), \tag{48}$$
$$j_{22_i} = -s(q_{3i} + \theta_i)(a_{2i}s(q_{2i}) + a_{1i}s(q_{1i} + q_{2i})), \tag{49}$$
$$j_{23_i} = -a_{1i}s(q_{3i} + \theta_i)s(q_{1i} + q_{2i}), \tag{50}$$
$$j_{31_i} = 0, \tag{51}$$
$$j_{32_i} = -a_{2i}s(\gamma_{3i})c(q_{2i}) - a_{1i}s(\gamma_{3i})c(q_{1i} + q_{2i}), \tag{52}$$
$$j_{33_i} = -a_{1i}s(\gamma_{3i})c(q_{1i} + q_{2i}). \tag{53}$$

Thus, the Jacobian matrix of the robot's body can be written as

$$J_b = \begin{bmatrix} J_{leg_1} & 0 & \dots & 0 \\ 0 & \ddots & \ddots & \vdots \\ \vdots & \ddots & \ddots & 0 \\ 0 & \dots & 0 & J_{leg_6} \end{bmatrix}. \tag{54}$$

The matrix $\mathbf{R}_b$, in Equation (9), is based on three successive rotations through Euler angles represented by

$$R_{\mathrm{b}} = \begin{bmatrix} c_\beta c_\varphi & c_\varphi s_\alpha s_\beta - c_\alpha s_\varphi & s_\alpha s_\varphi + c_\alpha c_\varphi s_\beta \\ c_\beta s_\varphi & c_\alpha c_\varphi + s_\alpha s_\beta s_\varphi & c_\alpha s_\beta s_\varphi \\ -s_\beta & c_\beta s_\alpha & c_\varphi c_\beta \end{bmatrix}. \tag{55}$$

Relating the angular velocities of the robot's body as a function of the Euler angles, result in

$$\frac{\partial \omega_{\mathrm{b}}}{\partial \dot{q}_{b_2}} = \begin{bmatrix} c_\beta c_\varphi & -s_\varphi & 0 \\ c_\beta s_\varphi & c_\varphi & 0 \\ -s_\beta & 0 & 1 \end{bmatrix}. \tag{56}$$

To relate the angular velocities of the robot's body with the velocities of the joints of the i-th leg. We use the matrix $J_{x_{1i}}$. Again, we stress that this matrix depends on the amount of stance legs. In our application, considering all the six legs as support we have

$$J_{x_1} = \begin{bmatrix} I & \mathbf{\Omega}_{leg_1} \\ \vdots & \vdots \\ I & \mathbf{\Omega}_{leg_i} \end{bmatrix} \in \mathbb{R}^{3i\times 6}. \tag{57}$$

Therefore,

$$\dot{q}_a = -J_b^{-1} \begin{bmatrix} I & \mathbf{\Omega}_{leg_1} \\ \vdots & \vdots \\ I & \mathbf{\Omega}_{leg_i} \end{bmatrix} \begin{bmatrix} I & 0 \\ 0 & \dfrac{\partial \omega_{\mathrm{b}}}{\partial \dot{q}_{b_2}} \end{bmatrix} \begin{bmatrix} v_{bx} \\ v_{by} \\ v_{bz} \\ \dot{\alpha} \\ \dot{\beta} \\ \dot{\varphi} \end{bmatrix}. \tag{58}$$

In walking robots, the complexity of the study of singularities increases, due to the amount of closed paths that may exist between the different arrangements of legs with the terrain. In general, authors usually divide the problem into two parts and details are beyond the scope of this work (Interested parties can search [57], [58]).

Being $\mathbf{J}_b \in \mathbb{R}^{3i\times 3i}$ is the Jacobian matrix of the robot body associated with the task space $\mathbf{q}_b$. Note that its $m \times n$ dimension changes according to the number of legs in the support phase. However, the matrix $\mathbf{J}_b$ is always square as a function of the number of support legs, and therefore, this matrix is singular only under the condition that its determinant is null. Thus

$$\det(\mathbf{J}_b) = \prod_{i=1}^{6} \det(\mathbf{J}_{leg_i}), \tag{59}$$

where, from (44),

$$\begin{aligned} \det(\mathbf{J}_{leg_i}) = {} & a_{1i}a_{2i}(s_{q_{1i}}(a_{3i} + c_{q_{2i}}(a_{1i}c_{q_{1i}} + a_{2i})) \\ & + s_{q_{2i}}(a_{1i}{c_{q_{1i}}}^2 - a_{1i}). \end{aligned} \tag{60}$$

In (60), singularities occur if $s_{q_{1i}} = \pm n\pi,\ \forall\, n \in \mathbb{N}$.

Singularity conditions appear in J_{x_2} depending on the adopted Euler angle convention. For the chosen rotation (see Equation (55)) the singularity condition occurs when $\cos\beta = \frac{\pi}{2}, \frac{3\pi}{2}, \dots (2n+1)\frac{\pi}{2},\ \forall\, n \in \mathbb{N}$. This configuration, practically improbable, corresponds to an orientation of the robot in the longitudinal axis completely vertical in relation to the support surface.

REFERENCES

[1] V. Dürr, L. M. Theunissen, C. J. Dallmann, T. Hoinville, and J. Schmitz, "Motor flexibility in insects: Adaptive coordination of limbs in locomotion and near-range exploration," *Behav. Ecol. Sociobiology*, vol. 72, no. 1, pp. 1–21, Jan. 2018.

[2] N. Gravish, D. Monaenkova, M. A. D. Goodisman, and D. I. Goldman, "Climbing, falling, and jamming during ant locomotion in confined environments," *Proc. Nat. Acad. Sci. USA*, vol. 110, no. 24, pp. 9746–9751, Jun. 2013.

[3] T. Wöhrl, L. Reinhardt, and R. Blickhan, "Propulsion in hexapod locomotion: How do desert ants traverse slopes?" *J. Experim. Biol.*, vol. 220, no. 9, pp. 1618–1625, Jan. 2017.

[4] T. Weihmann and R. Blickhan, "Comparing inclined locomotion in a ground-living and a climbing ant species: Sagittal plane kinematics," *J. Comparative Physiol. A*, vol. 195, no. 11, pp. 1011–1020, Nov. 2009.

[5] T. Seidl and R. Wehner, "Walking on inclines: How do desert ants monitor slope and step length," *Frontiers Zoology*, vol. 5, no. 1, pp. 1–15, 2008.

[6] S. E. Pfeffer, V. L. Wahl, and M. Wittlinger, "How to find home backwards? Locomotion and inter-leg coordination during rearward walking of *Cataglyphis fortis* desert ants," *J. Experim. Biol.*, vol. 219, no. 14, pp. 2110–2118, Jul. 2016.

[7] S. E. Pfeffer and M. Wittlinger, "Optic flow odometry operates independently of stride integration in carried ants," *Science*, vol. 353, no. 6304, pp. 1155–1157, Sep. 2016.

[8] K. Moll, F. Roces, and W. Federle, "How load-carrying ants avoid falling over: Mechanical stability during foraging in Atta vollenweideri grass-cutting ants," *PLoS ONE*, vol. 8, no. 1, Jan. 2013, Art. no. e52816.

[9] C. M. Harley, B. A. English, and R. E. Ritzmann, "Characterization of obstacle negotiation behaviors in the cockroach, Blaberus discoidalis," *J. Experim. Biol.*, vol. 212, no. 10, pp. 1463–1476, May 2009.

[10] S. Pick and R. Strauss, "Goal-driven behavioral adaptations in gap-climbing drosophila," *Current Biol.*, vol. 15, no. 16, pp. 1473–1478, Aug. 2005.

[11] J. Hwangbo, J. Lee, A. Dosovitskiy, D. Bellicoso, V. Tsounis, V. Koltun, and M. Hutter, "Learning agile and dynamic motor skills for legged robots," *Sci. Robot.*, vol. 4, no. 26, Jan. 2019, Art. no. eaau5872.

[12] E. Guizzo, "By leaps and bounds: An exclusive look at how Boston dynamics is redefining robot agility," *IEEE Spectr.*, vol. 56, no. 12, pp. 34–39, Dec. 2019.

[13] J. Hurst, "Walk this way: To be useful around people, robots need to learn how to move like we do," *IEEE Spectr.*, vol. 56, no. 3, pp. 30–51, Mar. 2019.

[14] M. Hörger, N. Kottege, T. Bandyopadhyay, A. Elfes, and P. Moghadam, "Real-time stabilisation for hexapod robots," in *Experimental Robotics*. Cham, Switzerland: Springer, 2016, pp. 729–744.

[15] D. Khudher and R. Powell, "Quadratic programming for inverse kinematics control of a hexapod robot with inequality constraints," in *Proc. Int. Conf. Robotics: Current Trends Future Challenges (RCTFC)*, Dec. 2016, pp. 1–5.

[16] S. Seok, D. J. Hyun, S. Park, D. Otten, and S. Kim, "A highly parallelized control system platform architecture using multicore CPU and FPGA for multi-DoF robots," in *Proc. IEEE Int. Conf. Robot. Autom. (ICRA)*, Jul. 2014, pp. 5414–5419.

[17] C. D. Bellicoso, F. Jenelten, P. Fankhauser, C. Gehring, J. Hwangbo, and M. Hutter, "Dynamic locomotion and whole-body control for quadrupedal robots," in *Proc. IEEE/RSJ Int. Conf. Intell. Robots Syst. (IROS)*, Jul. 2017, pp. 3359–3365.

[18] C. D. Bellicoso, F. Jenelten, C. Gehring, and M. Hutter, "Dynamic locomotion through online nonlinear motion optimization for quadrupedal robots," *IEEE Robot. Autom. Lett.*, vol. 3, no. 3, pp. 2261–2268, Jul. 2018.
[19] M. Focchi, V. Barasuol, M. Frigerio, D. G. Caldwell, and C. Semini, "Slip detection and recovery for quadruped robots," in *Robotics Research*. Cham, Switzerland: Springer, 2018, pp. 185–199.
[20] G. Bledt, M. J. Powell, B. Katz, J. Di Carlo, P. M. Wensing, and S. Kim, "MIT cheetah 3: Design and control of a robust, dynamic quadruped robot," in *Proc. IEEE/RSJ Int. Conf. Intell. Robots Syst. (IROS)*, Oct. 2018, pp. 2245–2252.
[21] M. Kalakrishnan, J. Buchli, P. Pastor, M. Mistry, and S. Schaal, "Fast, robust quadruped locomotion over challenging terrain," in *Proc. IEEE Int. Conf. Robot. Autom.*, Sep. 2010, pp. 2665–2670.
[22] R. Siegwart, I. R. Nourbakhsh, and D. Scaramuzza, *Introduction to Autonomous Mobile Robots*. Cambridge, MA, USA: MIT Press, 2011.
[23] M. Gorner, T. Wimbock, A. Baumann, M. Fuchs, T. Bahls, M. Grebenstein, C. Borst, J. Butterfass, and G. Hirzinger, "The DLR-crawler: A testbed for actively compliant hexapod walking based on the fingers of DLR-hand II," in *Proc. IEEE/RSJ Int. Conf. Intell. Robots Syst.*, Sep. 2008, pp. 1525–1531.
[24] D. Belter and K. Walas, "A compact walking robot–flexible research and development platform," in *Recent Advances in Automation, Robotics and Measuring Techniques*. Cham, Switzerland: Springer, 2014, pp. 343–352.
[25] D. Goldschmidt, F. Hesse, F. Wörgötter, and P. Manoonpong, "Biologically inspired reactive climbing behavior of hexapod robots, in 2012 IEEE," in *Proc. RSJ Int. Conf. Intell. Robots Syst.*, 2012, pp. 4632–4637.
[26] U. Saranli, M. Buehler, and D. E. Koditschek, "RHex: A simple and highly mobile hexapod robot," *Int. J. Robot. Res.*, vol. 20, no. 7, pp. 616–631, Jul. 2001.
[27] K. C. Galloway, G. C. Haynes, B. D. Ilhan, A. M. Johnson, R. Knopf, G. A. Lynch, B. N. Plotnick, M. White, and D. E. Koditschek, "X-RHex: A highly mobile hexapedal robot for sensorimotor tasks," Univ. Pennsylvania, Philadelphia, PA, USA, Tech. Rep., 2010.
[28] D. Belter, "Efficient modeling and evaluation of constraints in path planning for multi-legged walking robots," *IEEE Access*, vol. 7, pp. 107845–107862, 2019.
[29] W. Cheah, H. H. Khalili, F. Arvin, P. Green, S. Watson, and B. Lennox, "Advanced motions for hexapods," *Int. J. Adv. Robotic Syst.*, vol. 16, no. 2, pp. 1–13, 2019.
[30] A. Roennau, G. Heppner, M. Nowicki, and R. Dillmann, "LAURON V: A versatile six-legged walking robot with advanced maneuverability," in *Proc. IEEE/ASME Int. Conf. Adv. Intell. Mechatronics*, Jul. 2014, pp. 82–87.
[31] M. Bjelonic, N. Kottege, and P. Beckerle, "Proprioceptive control of an over-actuated hexapod robot in unstructured terrain," in *Proc. IEEE/RSJ Int. Conf. Intell. Robots Syst. (IROS)*, Oct. 2016, pp. 2042–2049.
[32] M. Bjelonic, T. Homberger, N. Kottege, P. Borges, M. Chli, and P. Beckerle, "Autonomous navigation of hexapod robots with vision-based controller adaptation," in *Proc. IEEE Int. Conf. Robot. Autom. (ICRA)*, May 2017, pp. 5561–5568.
[33] T. Homberger, M. Bjelonic, N. Kottege, and P. V. Borges, "Terrain-dependant control of hexapod robots using vision," in *Proc. Int. Symp. Experim. Robot.* Cham, Switzerland: Springer, 2017, pp. 92–102.
[34] S. Skaff, G. Kantor, D. Maiwand, and A. A. Rizzi, "Inertial navigation and visual line following for a dynamical hexapod robot," in *Proc. IEEE/RSJ Int. Conf. Intell. Robots Syst. (IROS)*, vol. 2, Sep. 2003, pp. 1808–1813.
[35] R. P. Bachega, R. Pires, and A. B. Campo, "Hardware configuration of hexapod robot to force feedback control development," in *Proc. 44th Southeastern Symp. Syst. Theory (SSST)*, Mar. 2012, pp. 115–120.
[36] R. Buchanan, L. Wellhausen, M. Bjelonic, T. Bandyopadhyay, N. Kottege, and M. Hutter, "Perceptive whole-body planning for multilegged robots in confined spaces," *J. Field Robot.*, vol. 38, no. 1, pp. 68–84, Jan. 2021.
[37] J. Denavit and R. S. Hartenberg, "A kinematic notation for lower-pair mechanisms based on matrices," *J. Appl. Mech.*, vol. 22, no. 2, pp. 215–221, Jun. 1955.
[38] P. I. Corke, "A simple and systematic approach to assigning Denavit–Hartenberg parameters," *IEEE Trans. Robot.*, vol. 23, no. 3, pp. 590–594, Jun. 2007.
[39] J. Paskarbeit, J. Schmitz, M. Schilling, and A. Schneider, "Layout and construction of a hexapod robot with increased mobility," in *Proc. 3rd IEEE RAS EMBS Int. Conf. Biomed. Robot. Biomechatronics*, Jul. 2010, pp. 621–625.
[40] D. Zhou, W. Zuo, X. Tang, J. Deng, and Y. Liu, "A multi-motion bionic soft hexapod robot driven by self-sensing controlled twisted artificial muscles," *Bioinspiration Biomimetics*, vol. 16, no. 4, Jul. 2021, Art. no. 045003.
[41] H. Li, C. Qi, F. Gao, X. Chen, Y. Zhao, and Z. Chen, "Mechanism design and workspace analysis of a hexapod robot," *Mechanism Mach. Theory*, vol. 174, Aug. 2022, Art. no. 104917.
[42] Y. Pan and F. Gao, "Payload capability analysis of a new kind of parallel leg hexapod walking robot," in *Proc. Int. Conf. Adv. Mech. Syst.*, Sep. 2013, pp. 541–544.
[43] K.-J. Huang, C.-K. Huang, and P.-C. Lin, "A simple running model with rolling contact and its role as a template for dynamic locomotion on a hexapod robot," *Bioinspiration Biomimetics*, vol. 9, no. 4, Oct. 2014, Art. no. 046004.
[44] G. Zhong, H. Deng, G. Xin, and H. Wang, "Dynamic hybrid control of a hexapod walking robot: Experimental verification," *IEEE Trans. Ind. Electron.*, vol. 63, no. 8, pp. 5001–5011, Aug. 2016.
[45] H. Ferrolho, W. Merkt, V. Ivan, W. Wolfslag, and S. Vijayakumar, "Optimizing dynamic trajectories for robustness to disturbances using polytopic projections," in *Proc. IEEE/RSJ Int. Conf. Intell. Robots Syst. (IROS)*, Oct. 2020, pp. 7477–7484.
[46] J. Chen, Z. Liang, Y. Zhu, and J. Zhao, "Improving kinematic flexibility and walking performance of a six-legged robot by rationally designing leg morphology," *J. Bionic Eng.*, vol. 16, no. 4, pp. 608–620, Jul. 2019.
[47] S.-S. Sun, *A Theoretical Study of Gaits for Legged Locomotion Systems*. Columbus, OH, USA: The Ohio State University, 1974.
[48] W. J. Davis, "Organizational concepts in the central motor networks of invertebrates," in *Neural Control of Locomotion*, R. M. Herman, S. Grillner, P. S. G. Stein, and D. G. Stuart, Eds. Boston, MA, USA: Springer, 1976, pp. 265–292, doi: 10.1007/978-1-4757-0964-3_11.
[49] S.-M. Song, *Kinematic Optimal Desing of a Six-Legged Walking Machine (Gait, Linkage Synthesis, Pantograph)*. Columbus, OH, USA: The Ohio State University, 1984.
[50] S.-M. Song and K. J. Waldron, *Machines That Walk: The Adaptive Suspension Vehicle*. Cambridge, MA, USA: MIT Press, 1989.
[51] S. Hirose, H. Tsukagoshi, and K. Yoneda, "Normalized energy stability margin: Generalized stability criterion for walking vehicles," in *Proc. Int. Conf. Climbing Walking Robots*, 1998, pp. 71–76.
[52] D. Messuri and C. Klein, "Automatic body regulation for maintaining stability of a legged vehicle during rough-terrain locomotion," *IEEE J. Robot. Autom.*, vol. RA-1, no. 3, pp. 132–141, Sep. 1985.
[53] S. Hirose, H. Tsukagoshi, and K. Yoneda, "Normalized energy stability margin and its contour of walking vehicles on rough terrain," in *Proc. IEEE Int. Conf. Robot. Autom. (ICRA)*, vol. 1, Jul. 2001, pp. 181–186.
[54] E. Garcia, J. Estremera, and P. G. de Santos, "A comparative study of stability margins for walking machines," *Robotica*, vol. 20, no. 6, pp. 595–606, Nov. 2002.
[55] A. Roennau, G. Heppner, M. Nowicki, J. M. Zöllner, and R. Dillmann, "Reactive posture behaviors for stable legged locomotion over steep inclines and large obstacles," in *Proc. IEEE/RSJ Int. Conf. Intell. Robots Syst.*, Jul. 2014, pp. 4888–4894.
[56] A. P. Bessonov and N. V. Umnov, "The analysis of gaits in six-legged vehicles according to their static stability," in *On Theory and Practice of Robots and Manipulators*, vol. 1. Vienna: Springer, 1974, pp. 1–10, doi: 10.1007/978-3-7091-2993-7_1.
[57] C. Gosselin and J. Angeles, "Singularity analysis of closed-loop kinematic chains," *IEEE Trans. Robot. Autom.*, vol. 6, no. 3, pp. 281–290, Jun. 1990.
[58] K. J. Waldron and K. H. Hunt, "Series-parallel dualities in actively coordinated mechanisms," *Int. J. Robot. Res.*, vol. 10, no. 5, pp. 473–480, Oct. 1991.

RAFAEL PEREIRA BACHEGA received the B.Sc. degree in control and automation technology and the M.S. degree in automation and process control from the Federal Institute of São Paulo (IFSP), Brazil, in 2007 and 2013, respectively. He is currently pursuing the Ph.D. degree in electrical engineering with an emphasis in automation and control with the University of São Paulo. He is also an Adjunct Professor with IFSP, on leave from Escola Politécnica, University of São Paulo. His research interests include biomimetic robotics, legged locomotion, motion planning, and force sensing.

GABRIEL PEREIRA DAS NEVES received the B.Sc., M.Sc., and Ph.D. degrees in electrical engineering with an emphasis in automation and control from Escola Politécnica, University of São Paulo, São Paulo, Brazil, in 2015, 2017, and 2021, respectively. Currently, he is an Assistant Professor with the Department of Engineering, Insper. His research involves mechatronics systems, robust control design, LMI, LPV, and model-free control.

ALEXANDRE BRINCALEPE CAMPO received the B.Sc. degree in electrical engineering with an emphasis on control and automation and the master's and Ph.D. degrees in control systems from the Escola Politécnica, University of São Paulo, in 1991, 1995, and 2001, respectively. In 2014, he developed senior internship research with Harvard University, USA. He is currently a Full Professor with the Federal Institute of Education, Science, and Technology of São Paulo (IFSP), where he is responsible for subjects in the control area of the control and automation engineering and electronic engineering course. He is a Coordinator of the Applied Control Laboratory (LCA), IFSP, as a Professor of lato-sensu postgraduate course in control and automation. He is a Founding Partner of Soft Grippers Company, which exclusively licensed the patent for a soft robotic grip developed at IFSP. He coordinates the implementation of iDEALAB, IFSP, LCA's innovation division. His research areas are innovation, control of dynamic systems, bioengineering, soft robotics, and control of magnetic levitation systems (MAGLEV).

BRUNO AUGUSTO ANGELICO received the B.Sc. degree in electrical engineering from the State University of Londrina, in 2003, and the M.S. and Ph.D. degrees in electrical engineering from the University of São Paulo, in 2005 and 2010, respectively. He was an Associate Professor with the Federal University of Technology—Paraná (UTFPR), Cornélio Procópio, from 2009 to 2013. Currently, he is an Associate Professor with the Department of Telecommunications and Control Engineering, Escola Politécnica, University of São Paulo. He has experience in electrical engineering, focusing on practical control applications and digital control.